Materials and Design 42 (2012) 321–326 (Accepted Version)

Pitting-induced hydrogen embrittlement of magnesium-aluminium alloy

M. Bobby Kannan[a*], W. Dietzel[b]

[a]*Discipline of Chemical Engineering, School of Engineering and Physical Sciences, James Cook University, Townsville, Queensland 4811, Australia*

[b]*Institute of Materials Research, Helmholtz-Zentrum Geesthacht, Geesthacht D-21502, Germany*

ABSTRACT

In this study, the pitting corrosion susceptibility and its role on the hydrogen embrittlement behavior of AZ80 magnesium alloy were studied using slow strain rate testing (SSRT), electrochemical technique and immersion test method. The electrochemical and immersion tests in chloride-containing solution revealed severe pitting corrosion in the alloy. The SSRT results of the alloy under continuously-exposed conditions in chloride-containing solution and in distilled water showed that the mechanical properties of the alloy deteriorated considerably in both the solutions. Pre-exposure of the alloy in distilled water did not show any considerable change in the mechanical properties of the alloy, however in chloride-containing solution a significant loss in the mechanical properties was noticed. Cleavage facets were observed in the vicinity of the localized attacked region of the alloy pre-exposed in chloride-containing solution. Interestingly, desiccating the pre-exposed (in chloride-containing solution) samples reduced the loss in the mechanical properties, which

* Corresponding author.
Tel.: +61 7 4781 5080; fax: +61 7 4781 6788; e-mail: bobby.mathan@jcu.edu.au

could be attributed to reversible hydrogen. Thus, the study suggests that pitting corrosion facilitates hydrogen entry into the alloy and causes hydrogen embrittlement.

Keywords: Magnesium alloy; Hydrogen embrittlement; Stress corrosion; Pitting corrosion

1. Introduction

The environment-assisted cracking (EAC) behavior of magnesium and its alloys has been studied over the past years. Generally, the EAC in magnesium and its alloys has been attributed to anodic-dissolution assisted cracking, i.e., stress corrosion cracking (SCC) and to hydrogen-assisted cracking caused by hydrogen embrittlement (HE). The anodic dissolution tendency of magnesium in aqueous environments is due to its high electronegative potential and to the fact that the corrosion product/film formed on magnesium is not protective, especially in chloride-containing environment. Hence, magnesium and its alloys are susceptible to localized corrosion, such as pitting, and to SCC in chloride-containing environment [1-4].

Magnesium dissolution in aqueous solution, an anodic reaction, is accompanied by a cathodic reaction, generally hydrogen evolution. It is widely cited that hydrogen plays a major role in the EAC of magnesium alloys [1,5]. However, the HE mechanism(s) are not clearly established. Lynch and Trevena [6] believed that in pure magnesium, hydrogen diffusion ahead of the crack tip causes HE. Based on theoretical extrapolation, Atrens et al. [7] suggested that the hydrogen diffusion coefficient in magnesium at ambient temperature is sufficient to allow for significant hydrogen transport ahead of stress corrosion cracks. Stampella et al. [8] reported that hydrogen entry into the pure magnesium is only possible when the hydrogen evolution reaction occurs on a film-free magnesium surface. In other words, hydrogen entry through $Mg(OH)_2$ passive film is highly unlikely. However, in the presence of

chloride ions the passive film is not stable, it dissolves [9]. Hence, presence of chloride ions in the solution can pave way for hydrogen entry into the alloy.

A study by Meletis and Hochman [10] on the EAC behavior of pure magnesium suggested that EAC was accompanied by hydrogen evolution and that cracking was initiated at corrosion pits. However, in the aluminium-containing AZ series magnesium alloys which are commercially popular, the nature of the protective film is different than that in pure magnesium. Fairman and Bray [11] proposed that two Al^{3+} ions are incorporated into the tetrahedral $Mg(OH)_2$ lattice by replacing three Mg^{2+} ions resulting in vacant lattice sites, and as a result a thicker film was formed on aluminium-containing magnesium alloy as compared to that in pure magnesium. Although aluminium addition to magnesium enhances the general corrosion resistance significantly, the pitting corrosion susceptibility is not completely inhibited [12]. Hence, in order to elucidate the role of pitting corrosion on the HE behaviour of magnesium-aluminium alloy, AZ80 magnesium alloy was examined using slow strain rate testing under different environmental conditions.

2. Experimental procedure

Extruded AZ80 alloy (Al-8.59, Zn-0.45, Mn-0.16, Fe-0.003, Mg – balance, all wt.%) was used in this study. The alloy was heat-treated to the F condition (stress relieved for 8 hours at 385°C prior to extrusion, aged for 16 hours at 420°C, cooled in air). The microstructure of the alloy was examined using an optical microscope. The specimens for the optical microscopy were prepared by standard metallographic procedures and were etched in a solution containing 3.5 g picric acid, 6.5 ml acetic acid, 20 ml water and 100 ml ethanol. A detailed study of the secondary phase particles distributed in the alloys was done using a scanning electron microscope (SEM) and an energy dispersive X-ray (EDX) analyser.

Immersion tests were carried out on flat samples with the dimension 20x20x5 mm. The samples were grinded with SiC paper up to 1200 grit and were cleaned with acetone prior to testing. The samples were immersed in 0.5 wt.% NaCl solution for 4 hours and 24 hours and then cleaned using chromic acid. Later, the samples were taken to SEM to identify the mode of corrosion.

The electrochemical corrosion behaviour of the alloy was studied using the potentiodynamic polarization technique. The experiments were carried out using a potentiostat and a typical three electrode system with platinum gauze as counter electrode, saturated calomel electrode (SCE) as reference electrode and the specimen as the working electrode. The samples were polished with SiC paper up to 1200 grit and were cleaned with acetone prior to testing. Potentiodynamic polarisation was carried out in 0.5 wt.% NaCl solution and in distilled water. Post-corrosion analysis was carried out on these samples using SEM.

The EAC behaviour of the alloy was studied using the slow strain rate testing (SSRT) method, according to ISO 7539-7 standard [13]. Round tensile specimens with gauge dimensions of 10 mm length and 5 mm diameter were used in this study. The sample preparation was similar to that for the electrochemical corrosion tests. In the SSRT tests, the samples were pulled at a strain rate of 10^{-6}/s in different environmental conditions, i.e., air, distilled water, 0.5 wt.% NaCl solution, pre-exposed to distilled water for different durations (24 hours and 48 hours) and then tested in air, and pre-exposed to 0.5 wt.% NaCl solution for different durations (24 hours and 48 hours) and then tested in air. Fracture surface analysis on the failed samples was done using SEM to identify the mode of cracking.

3. Results

3.1 Microstructure

Optical microstructure of AZ80 alloy showed fine grains and some random clusters of secondary phase particles (Fig. 1a). A higher magnification of the clusters revealed a lamellar structure of the particles (Fig. 1b). The grain boundaries were also decorated by secondary phase particles. EDX analysis showed that the precipitates in the grain and at the grain boundaries were rich in magnesium and aluminium, corresponding to $Mg_{17}Al_{12}$ (β phase).

3.2 Immersion test

The SEM micrographs of the alloy after immersion in 0.5 wt.-% NaCl solution for two different durations are shown in Fig. 2. The alloy immersed for 4 hours showed pitting corrosion and also some attack along the grain boundaries (Fig. 2a). The pit size was similar to the grain size of the alloy, which suggests two possible mechanisms: (i) complete dissolution of grains, or (ii) continuous attack along the grain boundaries leading to the falling out of the grains. Although a few small pits were evident in the grains, the latter mechanism appears to be more likely in creating large pits since grain boundary attack was predominant. The grains containing lamellar structure of β-precipitates showed selective dissolution of only the α-phase leaving behind the stable network of β-precipitates. The degree of attack in the alloy increased significantly when the alloy was immersed for a longer period, i.e., 24 hours (Fig. 2b). The pits had coalesced along the extrusion direction, creating trenches.

3.3 Potentiodyanamic polarisation

The polarization curve of the alloy obtained in 0.5 wt.% NaCl solution is shown in Fig. 3. The anodic curve of the alloy showed a break-down potential just

50 mV above the corrosion potential (E_{corr}). Generally, an observation of a break-down potential in the anodic curve is related to passive-film breakdown/pitting corrosion of the alloy. In order to confirm this, AZ80 alloy was tested in distilled water. The alloy showed no break-down potential in distilled water (Fig. 3), thereby confirming that the breakdown potential was an indication of the alloy`s susceptibility to pitting corrosion in chloride-containing environment. Further, the SEM micrographs of the sample after polarisation in 0.5 wt.% NaCl also showed large pits (Fig. 4a). A higher magnification of the corroded sample revealed a large number of small pits and coalescence of pits (Fig. 4b).

3.4 Slow strain rate testing

The SSRT data of AZ80 alloy tested in different environments, i.e., in air, distilled water and in 0.5 wt.-% NaCl solution is shown in Fig. 5. The alloy exhibited a strain to failure, ε_f, of 25 % and an UTS of 350 MPa when tested in air. In the tests in distilled water, the alloy showed significantly lower mechanical properties: ε_f = 11 % and UTS = 320 MPa. The mechanical properties further decreased in the presence of chloride (i.e., 0.5 wt.% NaCl): ε_f = 7 % and UTS = 290 MPa.

The SSRT data of AZ80 alloy tested in air after pre-exposure to distilled water and in 0.5 wt.-% NaCl for 24 hours period is shown in Fig. 6. The alloy pre-exposed to distilled water did not show any noticable difference in the mechanical properties from that of the air tested samples; accordingly, the pre-exposed alloy exhibted: ε_f = 25 % and UTS = 355 MPa. However, the alloy pre-exposure to 0.5wt.% NaCl solution showed a drastic loss in the mechanical properties. Thus, the alloy pre-exposed to 0.5wt.% NaCl solution exhibited: ε_f = 8 % and UTS = 300 MPa. In order to see whether there was any influence of increasing pre-exposure period, the samples

were pre-exposed to distilled water and 0.5wt.% NaCl solution for 48 hours. The alloy pre-exposed to distilled water did not show any significant change in the mechanical properties, i.e. ε_f = 24 % and UTS = 350 MPa, as compared to the 24 hours pre-exposed alloy. However, the mechanical properties of the alloy decreased marginally when pre-exposed to 0.5wt.% NaCl solution for 48 hours as compared to that of the 24 hours pre-exposed alloy. The pre-exposed alloy for 48 hours exhibited: ε_f = 7 % and UTS = 290 MPa.

3.5 Fractography

Fig. 7 shows representative fractographs of the SSRT samples tested in air, distilled water and in 0.5wt.% NaCl solution. As expected, the alloy tested in air showed typical ductile fracture features (Fig. 7a). In contrast, the alloy tested in distilled water showed a brittle failure (Fig. 7b). A higher magnification of the fracture surface revealed predominantly transgranular cracking with some secondary cracks (Fig. 7c). The alloy tested in 0.5 wt.% NaCl solution showed a different mode of failure. Noticeably, the edge of the fracture surface exhibited significant pitting corrosion (Fig. 7d). The circumference of the failed tensile sample revealed localized corrosion attack (Fig. 7e) similar to that of the flat samples immersed in 0.5wt.% NaCl solution for 24 hours (Fig. 2b). The fracture surface revealed a mixed-mode of failure, i.e. brittle features and a few fine dimples (Fig. 7f).

The fractographs of the alloy pre-exposed to distilled water and to 0.5 wt.% NaCl solution for 48 hours are shown in Fig. 8. Similar to the air tested sample (Fig. 7a) the fracture surface of the alloy which had been pre-exposed to distilled water showed typical ductile fracture features (Fig. 8a). However, the fracture surface of the alloy pre-exposed to 0.5 wt.% NaCl solution showed two distinct regions, i.e.

localized corrosion attack at the edge of the fracture surface and some brittle feature (Fig. 8b). Typical cleavage facets were observed in the vicinity of localized corrosion region (Fig. 8c,d).

4. Discussion

Specimens of AZ80 alloy showed drastic loss in the mechanical properties when being continuously immersed in distilled water during the SSRT test, whereas the alloy showed no significant change in the mechanical properties when the alloy was pre-exposed to distilled water and then SSRT tested. The reason for this different behavior of the alloy could be due to the pH change in the environment and the effect of slow-straining. Basically, dissolution of magnesium in aqueous solution increases the pH of the solution due to the reaction: $Mg + 2H_2O \rightarrow Mg(OH)_2 + H_2$ [14]. The neutral aqueous solution becomes alkaline very rapidly, i.e., the pH of the solution quickly reaches 9 and then slowly further increases with time. According to the Pourbaix diagram, magnesium hydroxide is stable at alkaline pH (above 9) [15]. In the case of the pre-exposure test in distilled water the increase in the pH due to initial dissolution of magnesium protects the alloy from further corrosion and hence does not affect the mechanical properties during SSRT testing in air. However, in the case of continuous exposure of the sample in distilled water during the SSRT testing, although the pH of the solution increases due to the initial dissolution of magnesium, the straining of the sample breaks the passive film. The process of passivation and film break-down occurs repeatedly. But, it should be noted that for magnesium and its alloys the magnesium dissolution/passivation which is an anodic reaction is accompanied by a hydrogen reduction reaction. Hence, hydrogen is readily available for diffusion into the metal which can then lead to hydrogen embrittlement. Accordingly, the fracture surface of the continuously-exposed sample showed typical

transgranular fracture, which is widely related to hydrogen-induced cracking [1]. Further, the secondary cracking observed on the fracture surface is another indication of hydrogen embrittlement. Hence, it can be stated that the loss in mechanical properties observed for the AZ80 alloy when SSRT tested in distilled water is due to hydrogen embrittlment.

In 0.5 wt.% NaCl solution the alloy showed a drastic loss in the mechanical properties in both continuously-exposed and pre-exposed conditions. The detrimental effect of chloride on the mechanical properties of the alloy was clearly evident when comparing the SSRT data of pre-exposed samples in 0.5 wt.% NaCl and in distilled water. Increase in the pre-exposure time in 0.5 wt.% NaCl showed a further loss in the mechanical properties of the alloy. Song et al. [16] reported that the degree of embrittlement increased in AZ31 alloy with increasing the pre-exposure time in chloride-containing solution. Winzer et al.[17] also reported that longer duration test produced larger SCC fracture surface as compared to shorter duration test for magnesium alloys. Stampella et al. [8] reported a grain size effect on the SCC behaviour of magnesium. They observed that fine-grained magnesium underwent transgranular cracking whereas larger grained magnesium exhibited a mixed-mode failure, i.e., transgranular and intergranular cracking. In the present study as well, AZ80 alloy, containing fine-grain size, underwent transgranular fracture.

The fracture surface of the alloy tested in 0.5 wt.% NaCl solution showed evidence of pitting corrosion at the edge of the fractured surface. Immersion tests and electrochemical experiments results of the alloy in 0.5 wt.-% NaCl solution also confirmed that the alloy was susceptible to pitting corrosion. Pardue et al. [18] reported that corrosion pits in AZ61 alloy induced cleavage cracks. However, the role of hydrogen due to pitting was not discussed. In order to confirm the role of hydrogen

and its relation to pitting in the HE behaviour of AZ80 alloy, the alloy was pre-exposed to 0.5 wt.-% NaCl for 24 hours (which was sufficient time for pitting corrosion to occur), then was desiccated for 7 days and then SSRT tested in air. The purpose of desiccating the samples was to allow some to the reversible hydrogen, if present, to diffuse out of the alloy. Interestingly, the alloy showed an increase in mechanical properties after the desiccated period as compared to the testing immediately after the pre-exposure in 0.5 wt.% NaCl. After desiccation, the alloy showed an ε_f of 10% and an UTS of 325 MPa. This confirms hydrogen entry into the alloy as a consequence of the pitting corrosion of the alloy. Stampella et al. [8] suggested that atomic hydrogen in solid solution of magnesium facilitates cleavage fracture. Recently, Uematsu et al. [19] observed that the crack propagation rate of AZ31 alloy increased with increase in hydrogen charging. Cheng et al. [20] reported that hydrogen enrichment and hydride formation in the β phase of AZ91 alloy caused SCC. Meletis and Hochman [10] reported cleavage features in the SCC of pure magnesium, which they attributed to an accumulation of atomic hydrogen/magnesium hydride formation. Winzer et al. [21] suggested that transgranular cracking in magnesium alloys is due to hydrogen concentration build up immediately behind the crack tip. In this study, the AZ80 alloy exposed to 0.5 wt.% NaCl solution showed typical cleavage facets which confirms the role of hydrogen in the failure mechanism.

To individually quantify the susceptibility of the alloy to EAC, HE and SCC (chloride-induced), their susceptibility indices were calculated as follows: I_{EAC} = mechanical properties in chloride-containing solution/ mechanical properties in air; I_{HE} = mechanical properties in distilled water/mechanical properties in air; I_{SCC} = mechanical properties in chloride-containing solution/mechanical properties in distilled water. A low index (EAC/HE/SCC) suggests high susceptibility of the alloy

to a particular environment, and when the index approaches unity it means that the alloy is highly resistant to the particular environment. The calculated indices presented in Fig. 9 suggest that both chloride and hydrogen played a role in the EAC susceptibility of the alloy and that in fact they had a synergetic effect.

5. Conclusions

A systematic study on the EAC behaviour of AZ80 magnesium alloy using SSRT testing in air, distilled water and 0.5 wt.% NaCl solution showed that the pitting susceptibility of the alloy plays a crucial role in the SCC and HE behaviour of the alloy. Pitting corrosion not only initiates SCC in the alloy, but also induces hydrogen into the alloy leading to HE.

References

[1] Winzer N, Atrens A, Song G, Ghali E, Dietzel W, Kainer KU, Hort N, Blawert C. A critical review of the stress corrosion cracking (SCC) of magnesium alloys Adv Eng Mater 2005;**7:**659-693.

[2] Bobby Kannan M, Dietzel W, Blawert C, Riekehr S, Kocak M. Stress corrosion cracking behavior of Nd:YAG laser butt welded AZ31 Mg sheet Mater Sci Eng A 2007;444: 220-226.

[3] Bobby Kannan M, Dietzel W, Zeng R, dos Santos JF, Zettler R. A study on the SCC susceptibility of friction stir welded AZ31 Mg sheet. Mater Sci Eng A 2007;460–461: 243-250.

[4] Bobby Kannan M, Dietzel W, Blawert C, Atrens A, Lyon P. Stress corrosion cracking of rare-earth-containing magnesium alloys ZE41, QE22, and Elektron 21 (EV31A) compared with AZ80. Mater Sci Eng A 2008;480:529-539.

[5] Bobby Kannan M, Dietzel W, Singh Raman RK, Lyon P. Hydrogen induced cracking in magnesium alloy. Scripta Materialia 2007; 57:579-581.

[6] Lynch S.P., Trevena P. Stress corrosion cracking and liquid metal embrittlement in pure magnesium. Corrosion (1988) 44 113-123.

[7] Atrens A, Winzer N, Song G, Dietzel W, Blawert C. Stress corrosion cracking and hydrogen diffusion in magnesium. Adv Eng Mater 2006;**7**8: 749-751.

[8] Stampella RS, Procter RPM, Ashworth V. Environmentally induced cracking of magnesium. Corros Sci 1984;24:325-341.

[9] Wang L, Zhang BP, Shinohara T. Corrosion behaviour of AZ91 magnesium alloy in dilute NaCl solutions. Materials and Design 2010;31:857-863.

[10] Meletis EI, Hochman RF. Crystallography of stress corrosion cracking in pure magnesium. Corrosion 1984;40:39-48.

[11] Fairman L, Bray FH. Intergranular stress-corrosion crack propagation in magnesium aluminium alloys. British Corrosion J 1971;6:170-174.

[12] Wang L, Shinohara T, Zhang BP. Corrosion behaviour of Mg, AZ31, and AZ91 alloys in dilute NaCl solutions. J Solid State Electrochem 2010;14:1897-1907.

[13] ISO 7539-9: 1989, Corrosion of metals and alloys –Stress corrosion cracking, Part 7: Slow strain rate testing, International Organization for Standardization, Geneva, Switzerland, 1989.

[14] Makar G.L., Kruger J. Corrosion of magnesium. Int. Mater. Rev. 38 (1993) 138-153.

[15] Pourbaix M. Atlas of Electrochemical equilibria in aqueous solutions. Pergamon Press, London, 1966 (Chapter IV).

[16] Song RG, Blawert C, Dietzel W, Atrens A. A study on stress corrosion cracking and hydrogen embrittlement of AZ31 magnesium alloy. Materials Science and Engineering A 2005;399:308-317.

[17] Winzer N, Atrens A, Dietzel W, Song G, Kainer KU. Comparison of the linearly increasing stress test and the constant extension rate test in the evaluation of transgranular stress corrosion cracking of magnesium. Materials Science and Engineering A 2008;472:97-106.

[18] Pardue WM, Beck FH, Fontana MG. Propagation of Stress-Corrosion Cracking in a Magnesium-Base Alloy as Determined by Several Techniques. Trans American Soc for Metals 1961;64: 539-548.

[19] Uematsu Y, Kakiuchi T, Nakajima M. Stress corrosion cracking behaviour of the wrought magnesium alloy AZ31 under controlled cathodic potentials. Materials Science and Engineering A 2012;531:171-177.

[20] Chen J, Wang J, Han E, Ke W. Effect of hydrogen on stress corrosion cracking of magnesium alloy in 0.1 M Na_2SO_4 solution. Materials Science and Engineering A 2008;488:428-434.

[21] Winzer N, Atrens A, Dietzel W, Song G, Kainer KU. Evaluation of the delayed hydride cracking mechanism for transgranular stress corrosion cracking of magnesium alloys. Materials Science and Engineering A 2007;466:18-31.

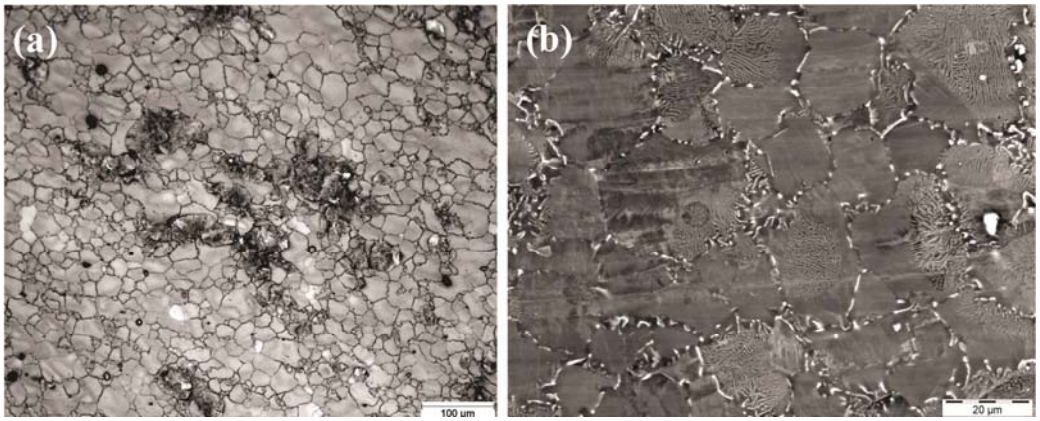

Fig. 1. Microstructures of AZ80 magnesium alloy: (a) optical micrograph shows the fine grains and clusters; and (b) a higher magnification SEM micrograph of the clusters reveal lamellar like structure of the particles.

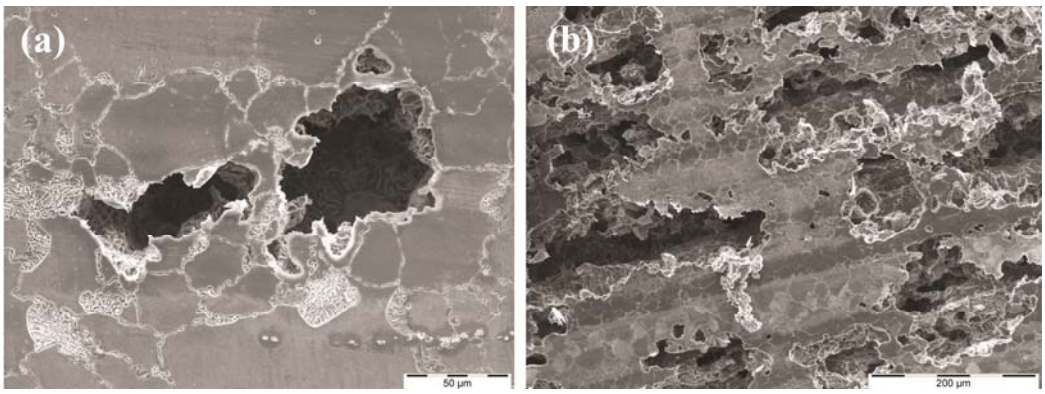

Fig. 2. SEM micrographs of AZ80 magnesium alloy after immersion in 0.5 wt.% NaCl solution: (a) 4 hours immersion shows large pits ; and (b) 24 hours immersion shows coalescence of pits forming trenches.

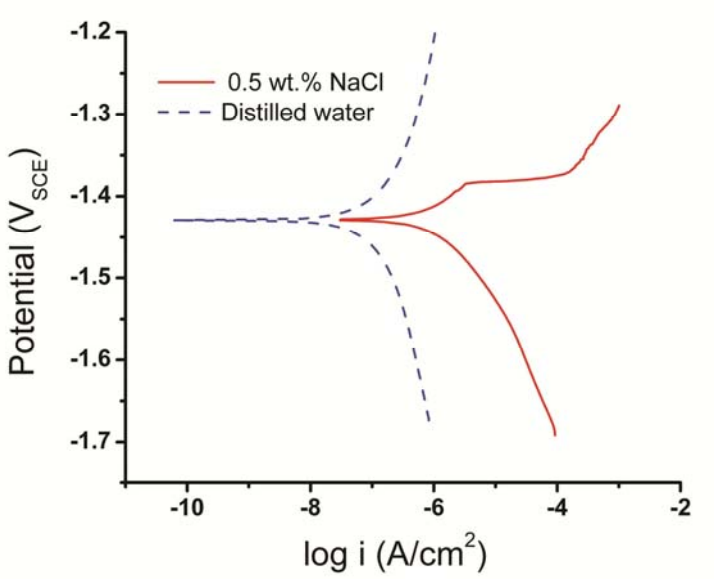

Fig. 3. Potentiodynamic polarisation of AZ80 magnesium alloy in 0.5 wt.% NaCl and in distilled water.

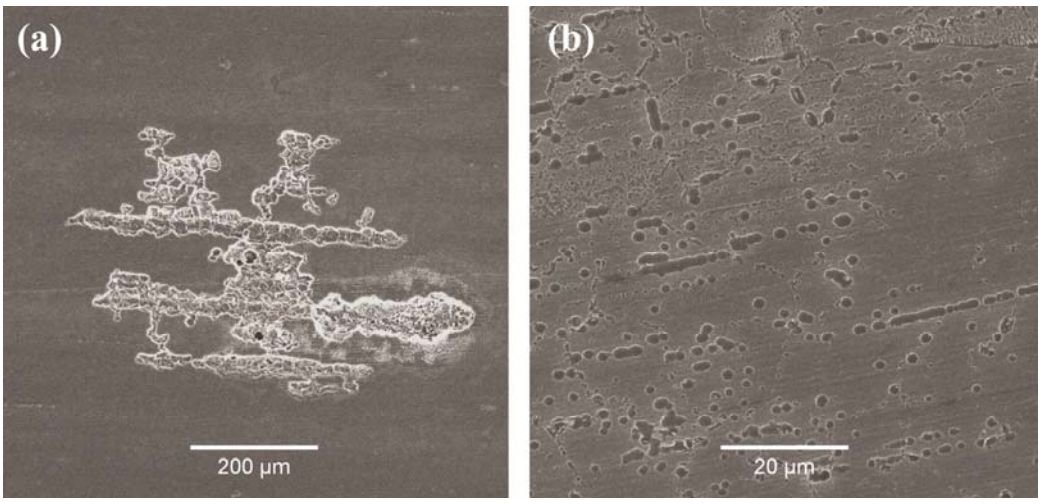

Fig. 4. Microstructures of AZ80 magnesium alloy after potentiodynamic polarization test in 0.5 wt.% NaCl solution: (a) large localized attack ; and (b) a large number of fine pits.

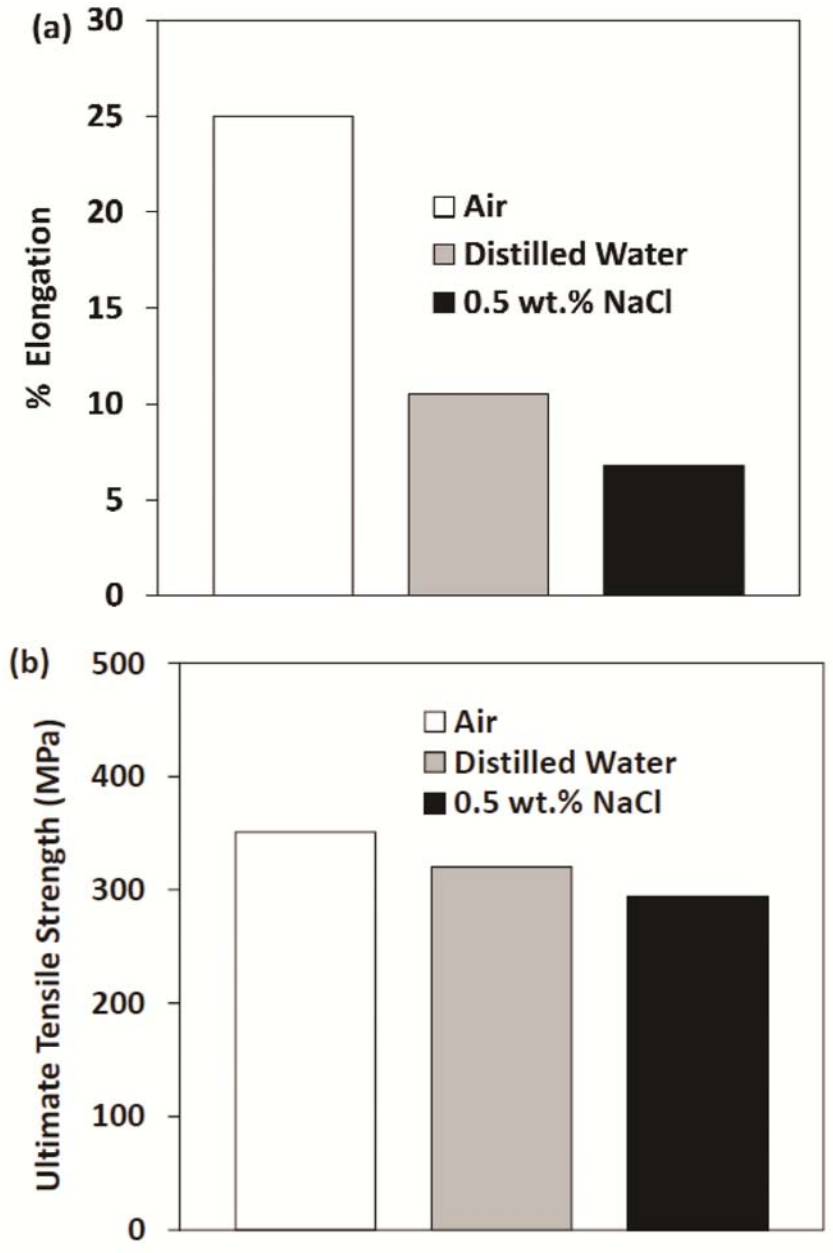

Fig. 5. SSRT data of AZ80 alloy exposed to different environments during the tests: (a) % Elongation and (b) Ultimate tensile strength.

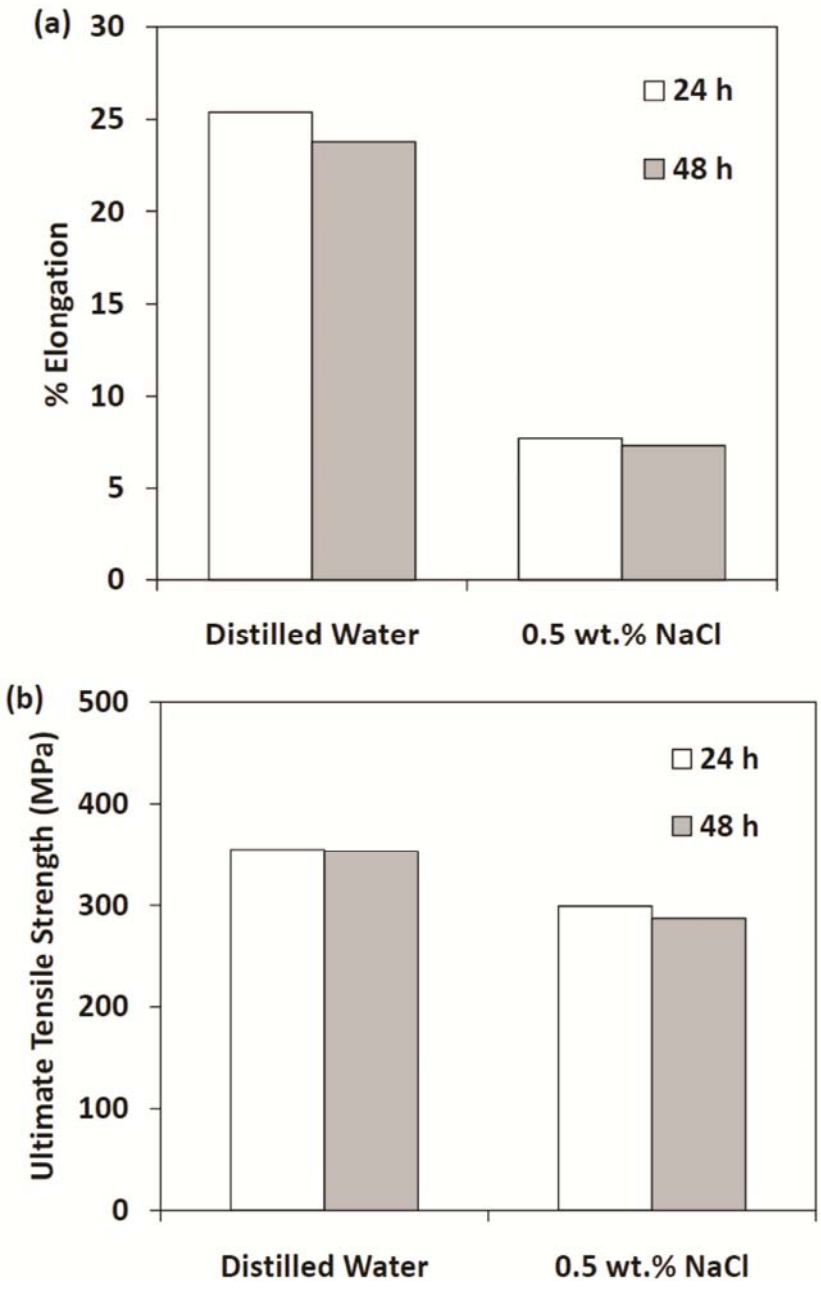

Fig. 6. SSRT data of AZ80 alloy pre-exposed to different environments for two different period of time: (a) % Elongation and (b) Ultimate tensile strength.

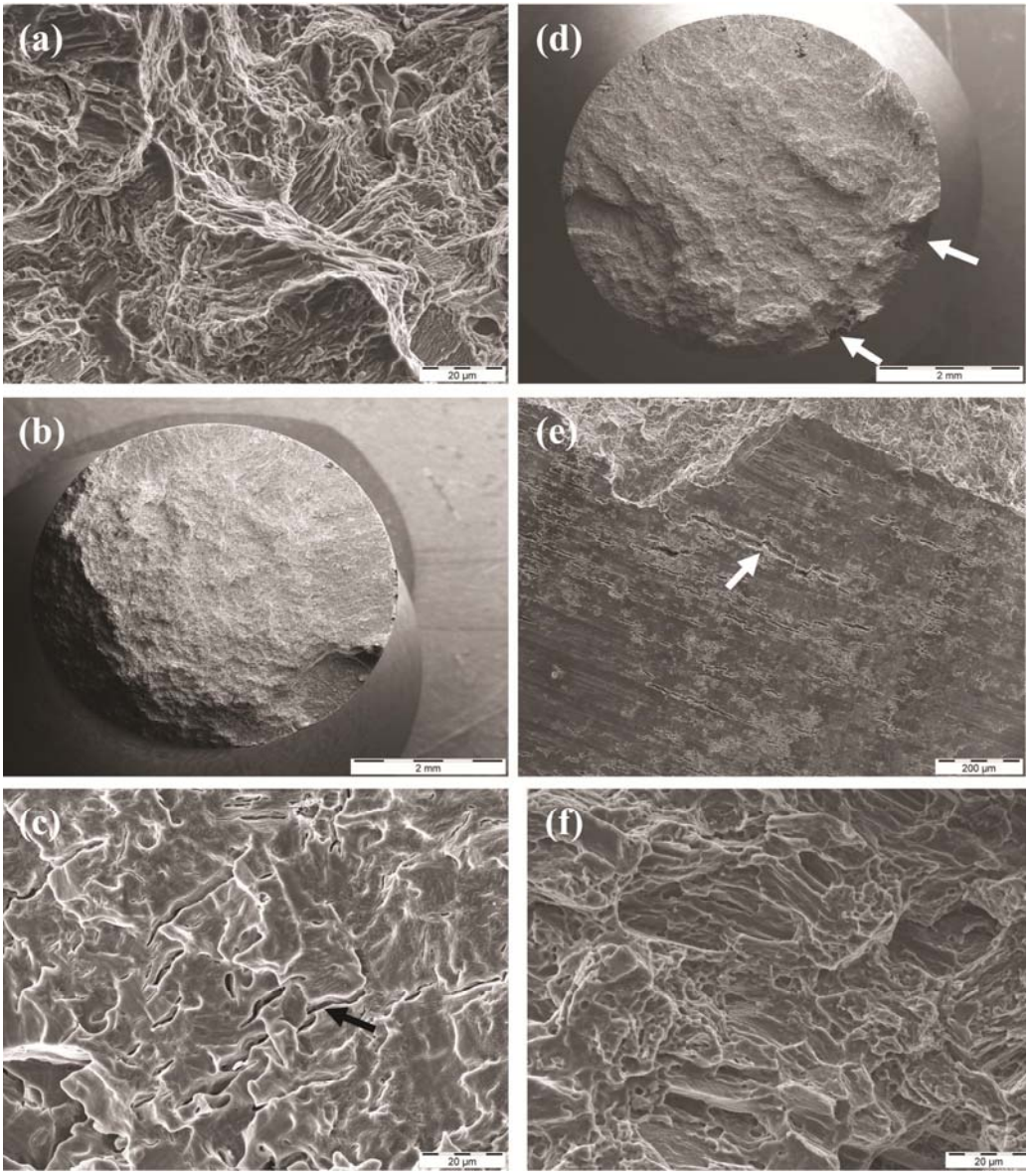

Fig. 7. Fracture surfaces of AZ80 alloy: (a) air – ductile fracture; (b) and (c) distilled water – (b) brittle fracture and (c) transgranular cracking and secondary cracks; (d), (e) and (f) 0.5wt.% NaCl solution - (d) brittle fracture and localized attack along the edge, (e) surface of tensile sample showing high localized attack, and (f) exhibits transgranular cleavage and a few fine dimples.

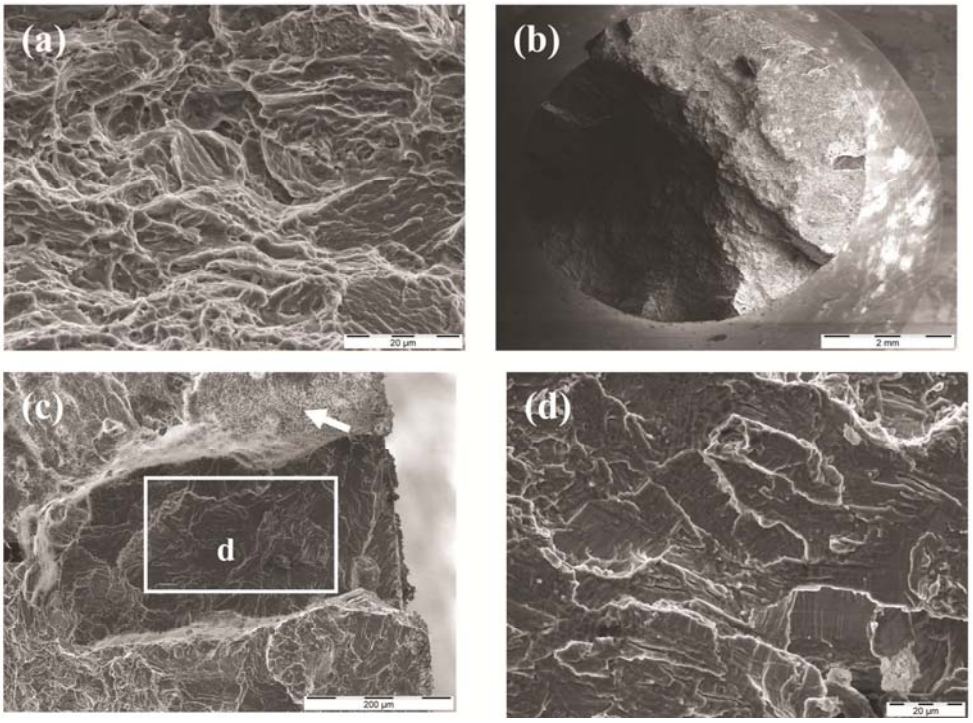

Fig. 8. Fracture surface of pre-exposed AZ80 alloy for 48h: (a) distilled water – ductile rupture; (b), (c) and (d) 0.5 wt.% NaCl solution – (b) overall fracture surface, (c) localized attack along the edge of the sample (arrow), and (d) typical cleavage facets.

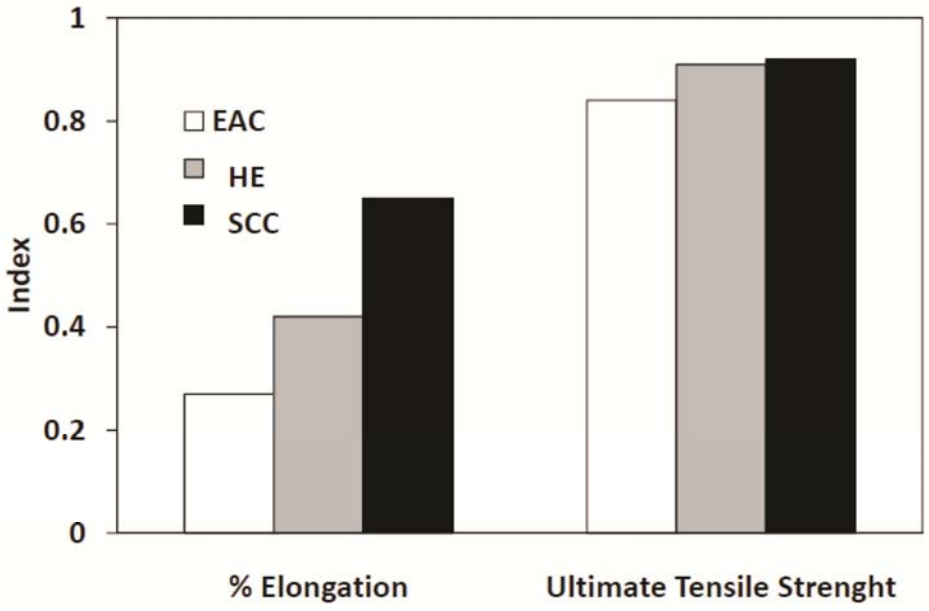

Fig. 9. Environmental assisted cracking, hydrogen embrittlement and stress corrosion cracking susceptibility indices for AZ80 alloy.